A dynamic electrically driven soft valve for control of soft hydraulic actuators

A dynamic electrically driven soft valve for control of soft hydraulic actuators

Siyi Xu[a,1], Yufeng Chen[b], Nak-seung P. Hyun[a], Kaitlyn P. Becker[a], and Robert J. Wood[a,1]

[a]John A. Paulson School of Engineering and Applied Sciences, Harvard University, Cambridge, MA 02134; and [b]Department of Electrical Engineering and Computer Science, Massachusetts Institute of Technology, Cambridge, MA 02139

Edited by Joseph M. DeSimone, Stanford University, Stanford, CA, and approved July 15, 2021 (received for review February 16, 2021)

Regulation systems for fluid-driven soft robots predominantly consist of inflexible and bulky components. These rigid structures considerably limit the adaptability and mobility of these robots. Soft valves in various forms for fluidic actuators have been developed, primarily fluidically or electrically driven. However, fluidic soft valves require external pressure sources that limit robot locomotion. State-of-the-art electrostatic valves are unable to modulate pressure beyond 3.5 kPa with a sufficient flow rate ($>$6 mL·min^{-1}). In this work, we present an electrically powered soft valve for hydraulic actuators with mesoscale channels based on a different class of ultrahigh-power density dynamic dielectric elastomer actuators. The dynamic dielectric elastomer actuators (DEAs) are actuated at 500 Hz or above. These DEAs generate 300% higher blocked force compared with the dynamic DEAs in previous works and their loaded power density reaches 290 W·kg^{-1} at operating conditions. The soft valves are developed with compact (7 mm tall) and lightweight (0.35 g) dynamic DEAs, and they allow effective control of up to 51 kPa of pressure and a 40 mL·min^{-1} flow rate with a response time less than 0.1 s. The valves can also tune flow rates based on their driving voltages. Using the DEA soft valves, we demonstrate control of hydraulic actuators of different volumes and achieve independent control of multiple actuators powered by a single pressure source. This compact and lightweight DEA valve is capable of unprecedented electrical control of hydraulic actuators, showing the potential for future onboard motion control of soft fluid-driven robots.

soft valves | dielectric elastomer actuators | fluidic actuators | soft robotics

Soft robots have been developed for an extensive variety of applications, including soft grippers (1–3), rehabilitative and assistive devices (4–8), and artificial muscles (9–12). Fluid-driven soft robots exhibit desirable properties for human–machine interactions (13, 14), delicate object manipulation (15–17), and operation in extreme environments (18, 19). Among these, soft actuators driven by pressurized liquids have shown robustness and high performance in versatile working environments (17, 20–23). Thus far, conventional rigid valves are the most prominent approach to control soft hydraulic robots (17, 19). These rigid systems contain major components made of inflexible materials, inducing potential risks of damaging delicate objects in their working environments. Furthermore, rigid valves are typically bulky and heavy ($>$100 g) relative to the soft actuators they control, significantly hindering the locomotion of soft robots. With these concerns, soft and lightweight valves are necessary to control soft hydraulic actuators and to achieve the future vision of onboard control of soft robots.

Many of the hydraulic actuators that have been developed in previous research have hundreds of microliters to tens of milliliters internal volume with mesoscale (0.1 to 1 mm) soft channels to deliver the working fluid (17, 24–26). To regulate these actuators, a soft valve should be able to control flows in mesoscale channels, regulate a pressure of at least 20 kPa, and provide a flow rate no lower than 6 mL·min^{-1}. Furthermore, hydraulic actuators with mesoscale channels could have an actuation time constant as low as 2 s (17, 25). A soft valve should have a response time shorter than the actuation time constant of the hydraulic actuators to achieve precise motion controls.

Numerous soft valves for microfluidic devices have been proposed, including the use of electrostatic forces (27–29), pressurized flow (30–33), and thermal energy (34–36). These valves have successfully demonstrated the control of flows in microchannels, but they cannot handle the flow rates required by many of the existing soft actuators (i.e., due to their fluidic impedance that is a consequence of their scale). Electrostatic microvalves utilize pressurized fluid as a dielectric material sandwiched between two soft electrode membranes. They require low operating voltages ($<$600 V) and have extremely short response times (in the range of milliseconds). Quake valves are fluidic valves consisting of multilayer structures with a flow channel and a control channel. Variants of Quake valves can provide control pressures higher than 100 kPa at 75 Hz or higher, but require external valves and regulated pressure sources to actuate the control channels (32, 37). Phase-change valves exploit phase transformations of thermal-responsive materials, blocking flows up to 276 kPa without any leakage (34, 35). While all these types of microfluidic valves have achieved notably high pressure control, they can regulate flow rates only in the range of nanoliters per minute (27). This shortcoming makes microvalves unsuitable for fluidic soft actuators with microliter to milliliter internal volumes.

Large-scale fluidic valves have been developed to increase the flow channel dimension while withstanding high pressures

Significance

Soft actuators have advantages over traditional rigid robots in various applications due to their robustness, low mechanical stiffness, and low weight. Thus far, conventional rigid valves are the most common approach to control hydraulic soft actuators. Although soft valves have been designed in various forms, they have not achieved the pressure or flow rate conditions as required by many existing hydraulic actuators. In this paper, we introduce an electrically driven soft valve using dynamic dielectric elastomer actuators (DEAs). These soft valves have a fast response time and are able to control fluidic pressure and flow rates that match the needs of hydraulic actuators with mesoscale channels. The DEA valves enable possibilities for soft onboard controls for future fluidic soft robots.

Author contributions: S.X. and R.J.W. designed research; S.X. and Y.C. performed research; K.P.B. contributed soft actuators/analytic tools; S.X., Y.C., and N.P.H. analyzed data; and S.X. and R.J.W. wrote the paper.

The authors declare no competing interest.

This article is a PNAS Direct Submission.

[1]To whom correspondence may be addressed. Email: sxu1@g.harvard.edu or rjwood@seas.harvard.edu.

This article contains supporting information online at https://www.pnas.org/lookup/suppl/doi:10.1073/pnas.2103198118/-/DCSupplemental.

Published August 20, 2021.

(25, 38, 39). However, these valves typically require heavy external pressure control hardware, limiting applicability to mobile robots. Electrically powered hydraulic valves are possible solutions to avoid immobile pressure sources. A powerful electroactive fluid valve built by Zatopa et al. (26) can regulate up to 264 kPa, but this valve is limited to electroactive fluids and cannot be applied to other actuators where water or other fluids serve as the working fluid (17, 40, 41). Quasistatic dielectric elastomer actuators (DEAs) are another option for electrical hydraulic valves. While a quasistatic DEA valve is applicable to a variety of pressurized fluids, state-of-the-art DEA valves have been unable to regulate a hydraulic actuator, owing to their limited controllable pressure (<3.5 kPa) and low bandwidths (<0.1 Hz) (42, 43).

In this work, we introduce an electrically powered dynamic DEA valve for hydraulic soft actuators (Fig. 1*A*). The dynamic DEA soft valve is able to regulate a hydraulic pressure up to 51 kPa and a maximum flow rate of $40\,\mathrm{mL}\cdot\mathrm{min}^{-1}$, with a response time less than 0.1 s. Furthermore, the proposed DEA valve can function as a proportional valve, tuning the hydraulic flow rate by varying its driving voltage. To achieve the desired performance with the proposed DEA valve, we first develop an ultrahigh-power density DEA that is lightweight (<350 mg), compact (7 mm active height), scalable, and highly robust to hundreds of thousands of working cycles. Second, we incorporate the DEA architecture with a soft channel, resulting in a 5.6-g soft valve for fluidic control. Our soft valve significantly outper-

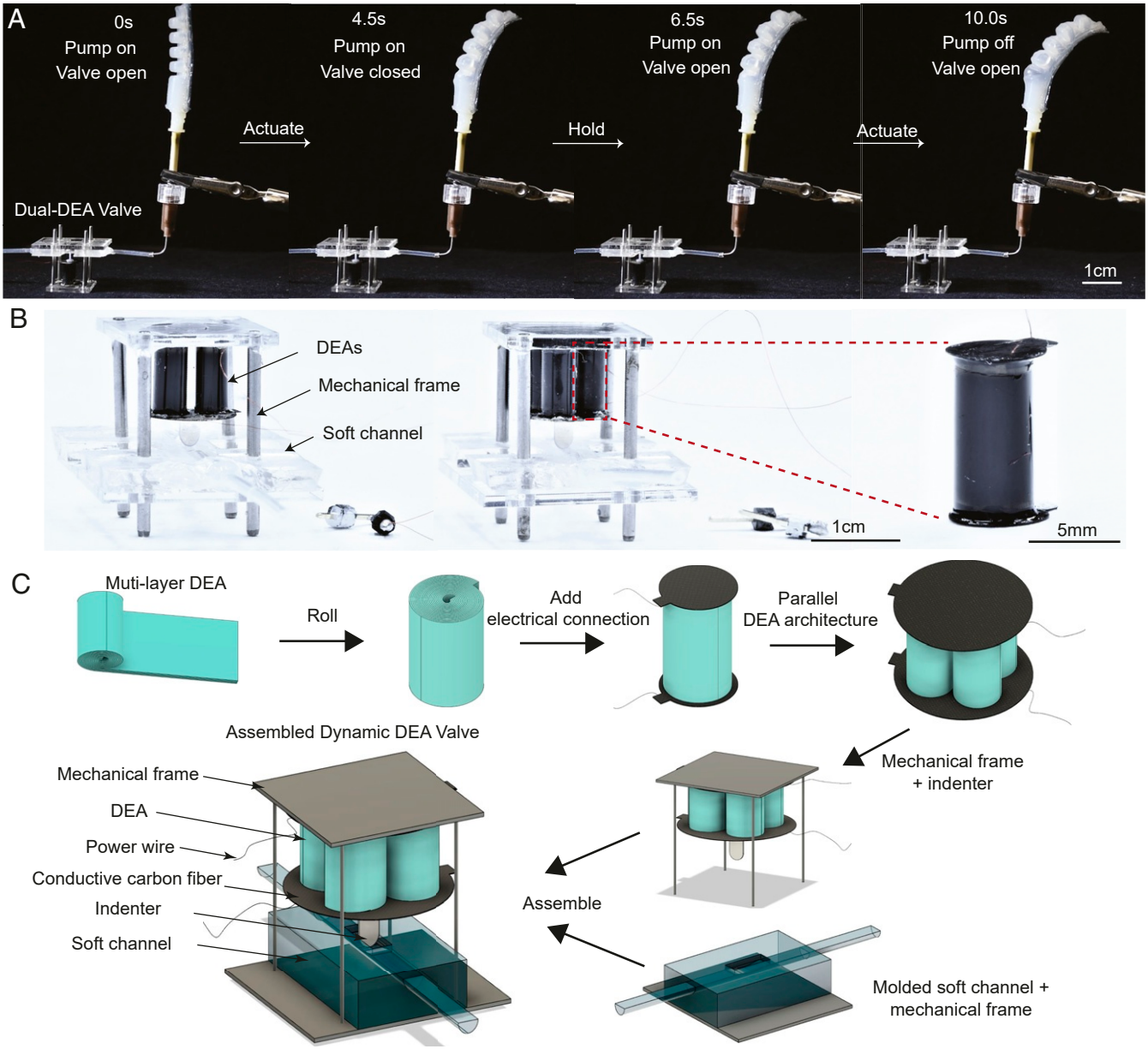

Fig. 1. Demonstration, design, and fabrication of soft dynamic DEA valves. (*A*) Demonstration of driving a fluidic soft actuator made of Ecoflex 0050 silicone with a dynamic DEA valve. The hydraulic pump is turned on at $t = 0$ s with the valve open. At $t = 4.5$ s, the valve is closed by operating the DEA at 1,800 V and 575 Hz. The valve remains closed for 2 s, which halts actuator inflation. The valve is open at $t = 6.5$s and the actuator continues to bend until $t = 10.0$ s when the pump is turned off. (*B*) Images of dual-DEA and triple-DEA valves. Each valve consists a dual- or a triple-DEA architecture, a soft channel, and a mechanical frame. (*C*) Schematic of the fabrication process of a parallel DEA architecture valve. The process involves the fabrication of a DEA and a soft channel and the integration of the two components with a mechanical frame.

forms conventional off-the-shelf rigid valves for soft fluid-driven actuators in many aspects. Table 1 compares the mass, power consumption, specific pressure, and specific flow rate of our DEA valve with those of a common mechanical valve (Swagelok KHR Series) and three miniature proportional solenoid valves (Enfield PFV Series, Kelly Pneumatics, and iQ Coral Series). Given these properties, our DEA valve is able to regulate hydraulic actuators with a variety of internal volumes as well as individual motion control for multiple actuators, representing advances for the electrical control of fluidic soft actuators.

Results

Operating Mechanism and Valve Design. Our DEA soft valve is composed of three major components: a soft channel, a DEA, and a mechanical frame (Fig. 1*B*). The soft channel is mounted to the bottom plate of the frame. The mechanical frame can be made of either rigid materials or soft elastomers and three-dimensional (3D) printed resins to provide reaction forces to counter the DEAs. In this paper, we demonstrate a valve with a simple frame composed of acrylic plates and metal pins. The DEA is designed as a multilayered cylindrical structure, with one end of the cylinder attached to the top plate of the mechanical frame and the other end free to deform the soft channel via an indenter. When the valve is at rest, the DEA and the soft channel are in contact and remain static. At this position, the valve is open, allowing free flow limited only by the geometry of the channel and the working fluid properties. When a sinusoidal voltage signal is applied to the DEA, an axial driving force is created due to the Maxwell stress generated between the soft electrodes. The magnitude of the Maxwell stress is proportional to the magnitude of the applied voltage squared: $P \propto \epsilon_e (\frac{V}{d})^2$, where ϵ_e is the dielectric constant of the elastomer, V is the voltage across the electrodes, and d is the elastomer thickness between two electrode layers. Under the driving force, the cylindrical DEA oscillates along its axial direction, fully or partially closing the valve, depending on the magnitude of the applied voltage.

For the valve to achieve the target pressure (>20 kPa), flow rate (>6 mL·min^{-1}), and response time (<0.1 s), the actuator must have a high energy density (>1 J·kg^{-1}) and a high actuation bandwidth (>10 Hz). We construct the DEA using a low viscoelasticity high dielectric strength silicone material, Elastosil P7670 (Wacker Chemical Corporation). This material causes the DEA to be underdamped, with a sharp free displacement resonant peak approximately six times larger than its static displacement. The channel material, on the other hand, is selected to be a dissipative acrylic elastomer, CN9021 (Startomer Company) (44), to avoid resonant behavior of the channel. The viscoelasticity discrepancy between the DEA silicone and the soft channel elastomer makes the valve a frequency–force leveraging system, converting a high-frequency, large displacement motion from DEAs into a high-force, low-frequency, and small displacement motion of the channel.

We develop a 2D dynamic mechanical model using constrained Lagrangian mechanics to understand and predict the interactions between the DEAs and the soft channels (*SI Appendix*, Fig. S1). In this model, we consider the DEA and the soft channel each to be a second-order linear time invariant (LTI) system consisting of an elastic spring, a dashpot, and a mass. We choose the channel to be 0.5 mm deep to ensure a sufficient flow rate under target hydraulic pressure (20 kPa). The pressure drop across the channel estimated with the Hagen–Poseuille equation is negligible (<0.5 kPa). We design the DEAs to be 7 mm tall based on the desired actuator stroke. From previous research, a 7-mm-tall dynamic rolled DEA can achieve a free displacement larger than our channel depth (45, 46). With our model, we simulate the channel displacement caused by the DEAs and compare it with the 0.5-mm channel depth to predict the valve behavior. From the model, a DEA roll made from a 50-mm-long 210-μm-thick multilayer sheet is able to generate a channel displacement of 0.4 mm (*SI Appendix*, Fig. S2). We combine two or three such DEA rolls in parallel to amplify the channel displacement to a minimum of 0.5 mm so that the valve can be fully closed. We design the soft channel cross-section to be an arc to minimize leakage when the valve is closed (*SI Appendix*, Fig. S3) (47). A 0.4-mm-thick indenter with the same arc-shaped profile as the channel is attached to the free end of the DEA. The small area of the indenter magnifies the output pressure from the DEAs, significantly increasing the controllable pressure range of the soft valve. The fabrication of the DEAs and valve assembly are depicted in Fig. 1*C*. A detailed description of the fabrication process is provided in *SI Appendix*.

High Power Density DEAs. To achieve high pressure and bandwidth control of hydraulic flows, the DEAs must have sufficient energy density and bandwidth. Many acrylic DEAs with high energy density (>4 J·kg^{-1}) have been developed in previous research (12, 48, 49), but these DEAs have limited bandwidth (<10 Hz) due to the viscoelasticity of the acrylic elastomer. For our DEA, we select a low-viscoelasticity and high dielectric strength silicone, Elastosil P7670, as the dielectric material. As a result, the DEAs can be driven at 500 Hz and above, reaching an estimated energy density of 4.6 J·kg^{-1} by virtue of the mechanical and electrical properties of the P7670 silicone. Elastosil P7670 has a low loss factor [$\tan(\delta)$] at 100 Hz of 0.095, approximately half of that of the commonly used highly elastic silicone Ecoflex 0030 (Smooth-On, Inc.). We characterize the frequency response of a P7670-based DEA with a 200V sinusoidal voltage input (Fig. 2*A*). The DEA free displacement shows a sharp resonant peak at 500 Hz with a quality factor Q of approximately 6. This Q factor is three times larger than that of the DEA developed in previous research (45, 46), suggesting a much larger resonant free displacement for our actuator. We operate the DEA near resonance to achieve high energy density operation when mounted in the soft valve. Furthermore, Elastosil P7670 has a high dielectric strength under alternating circuit (AC) signals. While previous dynamic DEAs could undergo unrecoverable failures at ∼45 V·m^{-1} AC (45, 46), our P7670 DEA could reach 66 V·m^{-1} without excessive self-clearing. Since the Maxwell stress is proportional to the square of applied voltage, increasing the drive voltage by a factor of 1.5 should improve the blocked force by a factor of 2.3, which further improves the DEA

Table 1. Valve property comparison

Valves	Mass, kg	Power consumption, W	Specific pressure, kPa·kg^{-1}	Specific flow rate, mL·min^{-1}·kg^{-1}
Dynamic DEA valve	0.0056	1.1	9,107.1	7,142.8
Mechanical valve, Swagelok KHR Series	2.75	—	1,253.5	3,636.4
Solenoid valve 1, Enfield PFV Series	0.155	2.1	2,580.6	6,193.5
Solenoid valve 2, Kelly Pneumatics	0.068	1.8	10,132.3	7,352.9
Solenoid valve 3, iQ Coral Series	0.521	6.0	287.9	—

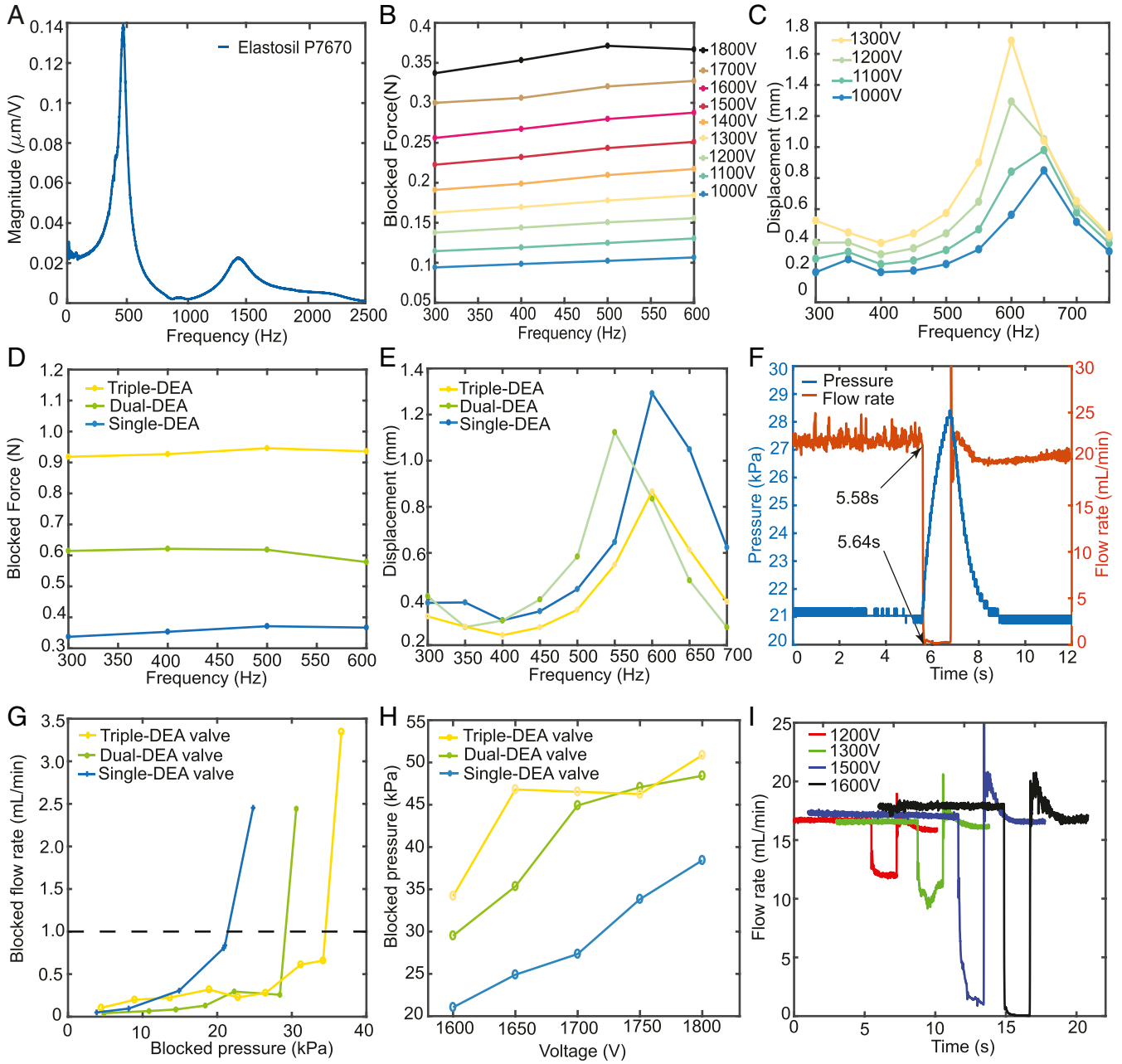

Fig. 2. High power density DEAs and dynamic soft valves characterization. (*A*) Frequency response of an 8-mm-tall DEA made of Elastosil P7670 silicone under 200 V excitation. (*B*) Blocked force of a single DEA as a function of frequency and driving voltage. (*C*) Free displacement of a single DEA as a function of frequency and driving voltage. (*D*) Blocked force comparison of a single DEA, a dual DEA, and a triple DEA operated under 1,800 V excitation. The blocked force of a triple DEA is ∼2.6 times higher than that of a single DEA. (*E*) Free displacement comparison of single DEA, dual DEA, and triple DEA operated at 1,200 V. (*F*) Synchronized pressure and flow rate response of a dual-DEA valve operated at 1,600 V and 575 Hz for 2 s. The valve blocks the channel 0.06 s after operation. (*G*) Blocked flow rates and blocked pressure of single-DEA, dual-DEA, and triple-DEA valves when operating at 1,600 V at resonance. We define the channel to be closed when the flow rate is lower than 1 mL·min^{-1} shown as a dashed line. (*H*) Blocked pressure, defined as the pressure when the channel is closed, of single-DEA, dual-DEA, and triple-DEA valves as a function of driving voltage. (*I*) Tunable flow rate of a dual-DEA valve operated at various voltages. A sudden reduction of the flow rate occurs as the DEA valve starts to operate, and the flow rates reach different levels based on the input voltage magnitude.

functionality. Considering the stability and lifetime of the actuator, we operate the DEA up to 1,800 V in this work.

The blocked force and free displacement of the DEAs are characterized with a force sensor (Nano-17; Titanium) and a vibrometer (PSV-500; Polytec), respectively. The blocked force is independent of frequency up to the actuator resonance (Fig. 2*B*). This is because our DEA's electrical time constant (0.06 ms) is more than 10 times smaller than the driving period associated with the highest operating frequency (1.7 ms). The DEA has a maximum blocked force of 0.37 N at 1,800 V and a resonant free displacement peak of 1.68 mm (24% strain) at 1,300 V, 600 Hz (Fig. 2 *B* and *C*). Considering that an electrical–mechanical instability may appear in DEAs without prestretch after 26% strain (50), we operate to a maximum of 1,300 V for free displacement measurement. Our DEAs achieve a power density of 697 W·kg^{-1} at 1,300 V (the power density is defined to be $\frac{F\delta}{2m}$, where

F is the blocked force, δ is the free displacement, and m is the mass), which is improved by ∼17% compared with the dynamically driven DEAs developed in previous research (45, 46). To explore the batch-to-batch variation of the DEAs, we fabricated three actuators and measured their blocked force up to 1,800 V and free displacements at 1,200 V (*SI Appendix*, Fig. S4). Due to fabrication defects, a variation of up to 28% of the free displacement and 5% of blocked force is observed between the three actuators.

Based on our model (*SI Appendix*, Fig. S2), a DEA with an active area of 7 × 90 mm is needed to generate a 0.5-mm channel displacement. Since a 7 × 50-mm DEA does not experience excessive self-clearing at 1,800 V, and increasing the active area is known to increase the likelihood of premature electrical failure (21, 51), we combine two or three such DEAs in parallel to amplify the DEA force output (Movie S1).

We analyze the free displacement, loaded displacement, blocked force, and loaded power density of a parallel DEA architecture as a function of the number of DEAs included. Without a load, a perfectly in-phase parallel DEA architecture is expected to have an aggregated blocked force, mass, and stiffness proportional to the number of DEAs, with the same free displacement. Therefore, the power density of an unloaded parallel DEA architecture should be theoretically invariant to the number of actuators. In practice, the power density decreases as the number of DEAs increases due to mismatches between the actuators caused by fabrication defects and the reduced resonant frequency caused by the inertia of the carbon fiber plate and the conductive adhesive used to combine the DEAs (*SI Appendix*, Fig. S4). Although experimentally the parallel arrangement reduces the free displacement and the average blocked force of each DEA (by ∼15%; Fig. 2 *D* and *E*), they are still able to achieve sufficient displacement to close the channel in our design.

In contrast, when a parallel DEA architecture is integrated into a valve, the loaded power density grows with the number of DEAs (*SI Appendix*, Fig. S2). Increasing the number of actuators increases the effective output impedance to better match that of the load, resulting in an increase in the loaded displacement. Since the blocked force, stiffness, and mass of a loaded parallel DEA architecture are proportional to the number of DEAs, the loaded power density grows as the number of DEAs increases (*SI Appendix*, Fig. S2). Assuming the effects of adding DEAs dominate, the loaded power density growth would eventually saturate when the loaded displacement approaches the free displacement. The experimentally measured power density of a loaded triple DEA driven with 1,800 V is ∼290 $W{\cdot}kg^{-1}$, 18% higher than a loaded single DEA driven under the same condition. Detailed characterization results of dual and triple DEAs (*SI Appendix*, Fig. S4) and their power density calculations are shown in *SI Appendix*.

High-Bandwidth DEA Valve for Regulating Hydraulic Flow. Taking advantage of the high power density DEA configuration, our dynamic valve can regulate greater than 10 times the pressure with a response time 50 times less than that of the DEA-based hydraulic valve in a previous research (42). The dynamic DEAs in our valve are designed with a high bandwidth (>500 Hz) to exploit resonance to increase their power density. We purposefully design the soft channel with a dissipative material such that the valve resembles the behavior of a regular quasistatic valve, despite the high-frequency input from the DEAs.

We characterize the DEA valve performance with a pressure sensor and a flow rate meter (*SI Appendix*, Fig. S5). When a DEA is integrated with a soft channel, the resonant displacement shown in Fig. 2*A* is reduced due to the channel impedance. To explore the frequency response of the DEAs under loaded conditions, we measure the flow rate variation in the channel at different driving frequencies. Lower DEA loaded displacement leads to less effective flow rate modulation. Based on the flow rate response to frequencies, we choose to operate the single-, dual-, and triple-DEA valves at 575, 575, and 525 Hz, respectively (*SI Appendix*, Fig. S6).

We define the valve to be closed when the flow rate is less than 1 $mL{\cdot}min^{-1}$—at this rate flow can be barely observed. We similarly define the corresponding pressure to be the valve blocked pressure. As shown in Fig. 2*F*, a dual-DEA valve can be closed when driven at 1,600 V, reducing the flow rate from 20 $mL{\cdot}min^{-1}$ to 0.1 $mL{\cdot}min^{-1}$ within 0.06 s. The valve stays closed with a flow rate lower than 0.4 $mL{\cdot}min^{-1}$ until it is released after 2 s. During operation, the valve reaches a blocked pressure of 28.5 kPa. The blocked pressure could be improved by increasing the driving voltage and the number of DEAs in the parallel architecture (Fig. 2 *G* and *H*). A triple-DEA valve operated at 1,800 V can achieve a blocked pressure of 51 kPa with an open valve flow rate of 40 $mL{\cdot}min^{-1}$ (*SI Appendix*, Fig. S7). The discrepancy between our experimental results and model predictions is less than 10% (*SI Appendix*, Fig. S2).

Furthermore, the dynamic DEA valve is able to tune the flow rate as a function of the input voltage magnitude. We demonstrate flow rate control by adjusting a dual-DEA valve input voltage from 1,200 to 1,600 V (Fig. 2*I*; *SI Appendix*, Fig. S8; and Movie S2). At 1,200 V excitation, the flow rate is reduced by ∼25% compared with the open valve flow. As the input voltage is gradually increased to 1,300, 1,500, and 1,600 V, the flow rates are ∼60, 20, and 0% of the free flow, respectively. This voltage-dependent flow rate makes the valve functionally equivalent to a proportional valve. We leverage this capability in the following section.

Our DEA valves convert electrical energy to mechanical energy. The dynamic DEA valve requires higher current input (20 mA) and consumes more power (1.1 W) than quasistatic DEA valves and exhibits a lower efficiency (42, 43), but provides a shorter response time (<0.1 s) and higher blocked pressure. Compared with previous research on dynamic DEAs that have less than 5.6% transduction efficiencies (46, 52), our triple-DEA valve has an efficiency of 9% (*SI Appendix*, Fig. S9). A detailed calculation of the power consumption and efficiency is provided in *SI Appendix*.

Macroscale Soft Actuator Control. The DEA valve is capable of controlling hydraulic actuators with a wide range of volumes and actuation times. We fabricated a bellows-shaped actuator based on prior designs using the silicone Ecoflex 0050 (Smooth-On, Inc.) (15). Its actuation volume—the differential volume from the rest position to the maximum deformation—is ∼4 mL. We connected the actuator to our DEA valve and a hydraulic pump to build a complete hydraulic system (Fig. 3*A*). This system has an approximate actuation time of 20 s—the time required for the actuator to reach maximum bending angle from the rest position. The actuation time is determined by the pump operation pressure, open-valve flow rate, the actuator stiffness, and the actuation volume. We pressurized the actuator with the pump from a neutral vertical position 0° to a 45° bending angle and released it to the original position. The working fluid flowed back to the pump under ambient pressure and gravity when the pump was turned off. This sequence was repeated three times and was controlled with the DEA valve at rest, operated at 1,800 and 1,400 V for each cycle (Fig. 3 *A*–*C* and Movie S3). In the second and third cycles, the hydraulic actuator has an initial position of 6.0° and 2.3°, respectively, due to incomplete deflation from the previous motion cycle. This variation causes a 2.4° bending angle difference among these cycles when the DEA valve starts to operate. However, the bending angle does not affect the control of the actuator in our demonstration, and it is

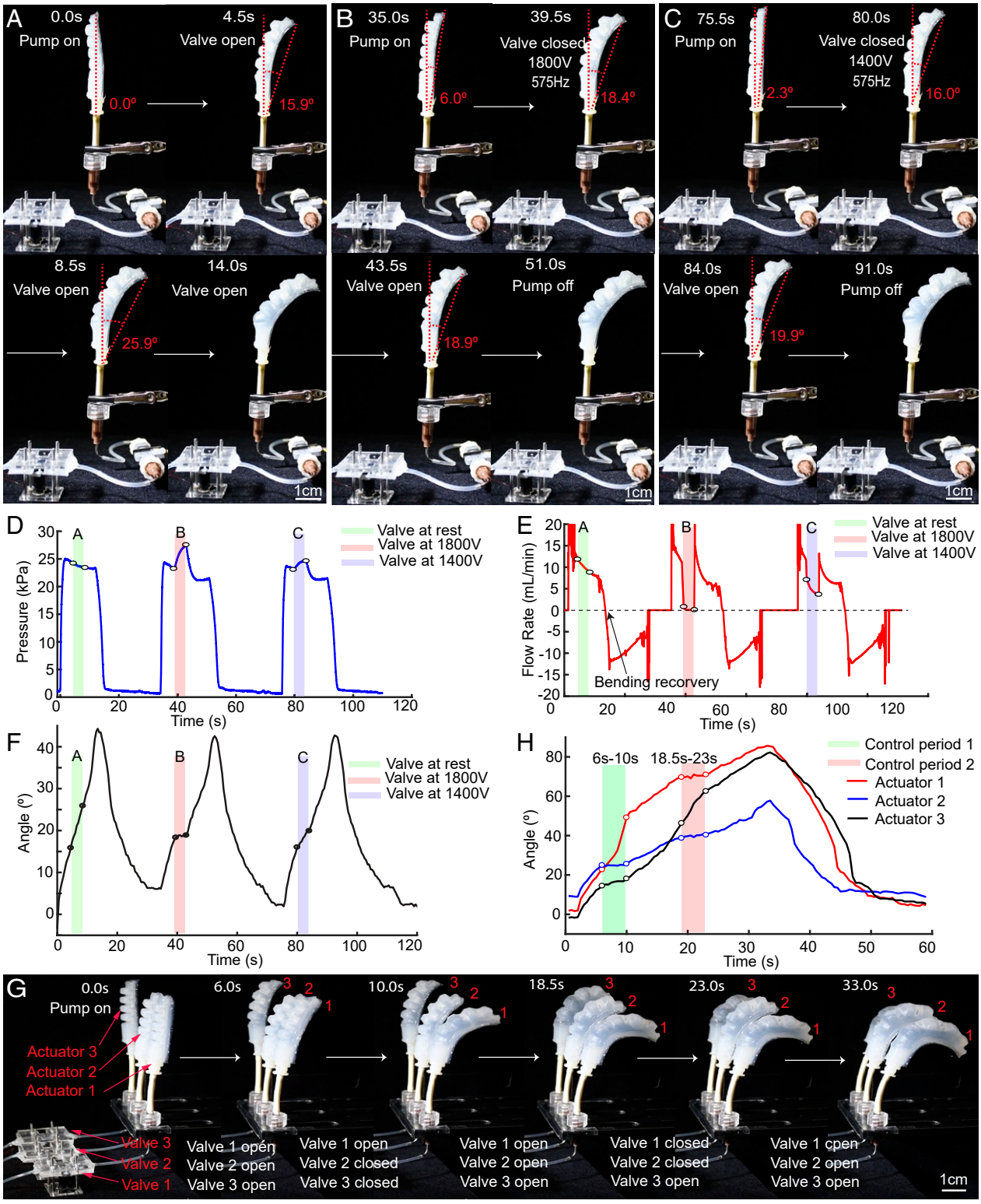

Fig. 3. Demonstrations of the DEA valves controlling macroscale hydraulic soft actuators. (*A*) Bending motion of a hydraulic actuator when a dual-DEA valve is at rest. (*B*) Bending motion of a hydraulic actuator when controlled by a dual-DEA valve at 1,800 V and 575 Hz. The valve is turned on at t = 39.5 s and turned off at t = 43.5 s. (*C*) Decelerated bending of a hydraulic actuator controlled by a dual-DEA valve at 1,400 V and 575 Hz. The valve is turned on at t = 80 s and turned off at t = 84 s. (*D*) DEA valve pressure response under the three operation conditions in *A*–*C*. The highlighted green, red, and purple areas correspond to the pressure change during the valve operation periods in *A*, *B*, and *C*, respectively. (*E*) DEA valve flow rate response under the three operation conditions in *A*–*C*. The highlighted green, red, and purple areas correspond to the flow rate change during the valve operation periods in *A*, *B*, and *C*, respectively. (*F*) Hydraulic actuator bending angle during the three operation cycles in *A*–*C*. The highlighted green, red, and purple areas correspond to the bending angle during the valve operation periods in *A*, *B*, and *C*, respectively. (*G*) Bending motions of three hydraulic actuators with a common input controlled by multiple DEA valves operated in parallel. (*H*) Bending angles of hydraulic actuators 1, 2, and 3, each controlled by a DEA valve. The highlighted green and red areas correspond to the bending angles during the first (6 to 10 s) and second (18.5 to 23 s) control periods in *G*, respectively.

possible to compensate for these offsets using feedback control (e.g., embedded soft or external motion sensors). Fig. 3 *D–F* shows the actuator's pressure, flow rate, and bending angle for the three cycles. The highlighted green, red, and blue areas represent the valve's operating period within each bending cycle. In the first cycle, the DEA valve was at rest. The actuator's bending angle increased from 15.9° to 25.9° at a speed of $2.5°\cdot s^{-1}$ (Fig. 3*F*, green area). This motion was substantially slowed down to $0.975°\cdot s^{-1}$ in the third cycle when the valve was driven at 1,400 V (Fig. 3*F*, purple area). During deceleration, the flow rate was decreased by 8 $mL\cdot min^{-1}$, accompanied by a 1.6-kPa increase in pressure (Fig. 3 *D* and *E*, purple areas). In the second cycle, the valve was operated at 1,800 V. It successfully stopped the actuator's motion by limiting the flow rate under 1 $mL\cdot min^{-1}$. The actuator was controlled to stop with a negligible speed of $0.125°\cdot s^{-1}$ (Fig. 3*F*, red area). The pressure increase during the second cycle was ∼4.5 kPa, about three times larger than that during the deceleration period in the third cycle (Fig. 3*D*, red area). To test the repeatability of the hydraulic system, we performed cyclic controlled stop experiments and drove the dual-DEA valve for 2 s each time. The controlled stop motion was able to repeat for 35 cycles. After that, the flow rate with the valve closed rose above 1 $mL\cdot min^{-1}$ (the defined blocked flow rate), and the actuator bending motion could no longer be fully stopped. This is primarily caused by wearing of the channel elastomer under high-frequency forces. We observed damage at the channel edge, which we believe caused the leak of the working fluid. To improve the lifetime of the system, more robust channel materials with similar mechanical properties (viscoelasticity, Young's modulus) to those of the CN9021 elastomer could be used. In addition, misalignment occurred between the DEA pinch tip and the channel due to high-frequency oscillation. We realigned the channel after 25 cycles to maintain the blocked flow rate below 1 $mL\cdot min^{-1}$. The flow rate and the hydraulic actuator bending angle are shown in *SI Appendix*, Fig. S10.

Furthermore, the valve's rigid mechanical frame could be replaced with soft materials, which will enable a more homogeneous integration with soft systems. To demonstrate this, we fabricated a dual-DEA valve with a soft mechanical frame (5:1 Sylgard 184 top and bottom plates and 3D-printed rods) and integrated this with the DEA valve actuators. The soft-frame dual-DEA valve performed equally well to the rigid valve, with a blocked pressure of 49.7 kPa driven at 1,800 V at resonance (48.4 kPa for a rigid-frame dual-DEA valve at the same driving condition). Additionally, the soft-frame DEA valve successfully demonstrated control of the macroscale hydraulic actuator motion when operated at 1,800 V at resonance (Movie S4). These stopped and deceleration motions demonstrate effective voltage-dependent control of a single macroscale hydraulic actuator with our DEA valve.

Control of Multiple Soft Actuators. To demonstrate multiactuator control with DEA valves, we operated three sets of actuator-valve systems attached to the same hydraulic pressure source (Fig. 3 *G* and *H* and Movie S5). We started with the pump at rest and the valves open for all three actuators (labeled actuators 1, 2, and 3). After turning on the pump for 6.0 s, we operated valves 2 and 3 at 1,800 V for 4 s. During this time, actuator 1 continued its bending motion while actuators 2 and 3 were held still (green highlighted area in Fig. 3*H*). In the second control period (red highlighted area in Fig. 3*H*), we closed valves 1 and 2 but left valve 3 open. During this cycle, actuator 2 was stopped together with actuator 1 while actuator 3 continued with its bending motion. With several valves operated in parallel, we achieve separate control of multiple actuators in a series of complex bending sequences.

High-Bandwidth Small-Volume Soft Actuator Control. The actuator volume is a dominating factor in determining the actuation speed. In addition to testing a macroscale actuator, we also fabricated a 100-mL volume actuator (53) with Ecoflex 0050. Similar to the control of larger actuators, we connected the small actuator to a dual-DEA valve and a pump. This hydraulic system has a less than 2-s actuation time, ∼10% that of the macroscale fluidic actuators. We initiated the operation with the actuator at a neutral vertical position. A comparison of the actuator positions with and without DEA valve control is shown in Fig. 4 *A* and *B*. The actuator bent at a speed of $75°\cdot s^{-1}$ with the DEA valve at rest and took 1.93 s to reach its maximum bending angle of 145.5°. As we operated the valve under 1,800-V excitation at 1.36 s, the actuator was stopped at the position of 81.7° for 1.8 s with less than 3% variation of the bending range (Fig. 4*C* and Movie S6). The corresponding flow rate response is shown in Fig. 4 *D* and *E*. The DEA valve limited the flow rate from 4.7 $mL\cdot min^{-1}$ to less than 1 $mL\cdot min^{-1}$ in 0.07 s. The valve response time is less than 1/10th the actuation time of the actuators described above.

Discussion

Our dynamic DEA valve controls up to 51 kPa of hydraulic pressure with a 40 $mL\cdot min^{-1}$ flow rate and a response time less than 0.1 s by utilizing an ultrahigh-power density DEA as its core. The viscoelasticity distinction between the DEA material and the soft channel elastomer is a critical factor of the dynamic valve. We explored the material properties of the DEA silicone Elastosil P7670 and channel acrylic elastomer CN9021 with a dynamic mechanical analyzer (DMA) (TA Instruments). We also tested the properties of the commonly used Ecoflex 0030 as a comparison (Table 2). We measured the loss factor $\tan(\delta)$ of each material up to 100 Hz and predicted their values at 600 Hz with a linear extrapolation. At 600 Hz, the estimated $\tan(\delta)$ of Elastosil P7670 is approximately eight times smaller than that of CZ9021, but is very close to that of Ecoflex 0030. To illustrate the effect of material properties on valve performance, we simulate the deformations of an Ecoflex 0030 channel and a CZ9021 channel when operating a triple-DEA valve at 1,800 V, 575 Hz. While the highly elastic Ecoflex 0030 channel deforms only by 0.34 mm, the CZ9021 channel is able to reach a displacement of 0.54 mm (*SI Appendix*, Fig. S10).

Another decisive factor of the valve performance is the use of dynamic DEAs. Our DEA has a high energy density of 4.6 $J\cdot kg^{-1}$ when operated above 500 Hz, owing to the large quality factor and the high dielectric strength under AC signals of the Elastosil P7670 silicone. Furthermore, we find the breakdown voltages of dielectric elastomers under AC are always higher than those at direct current (DC). Most elastomers have dielectric strengths lower than 35 $V\cdot\mu m^{-1}$ at DC (42, 43, 50); however, Elastosil P7670 could reach 66 $V\cdot\mu m^{-1}$ under AC excitation. This is primarily because of the short time duration that the elastomer experiences high voltages within each oscillation cycle. This property improves the driving voltage from 1,000 to 1,800 V, which results in an ∼19% improvement on the channel displacement from the DEAs (*SI Appendix*, Fig. S10). When the DEA valves are driven quasistatically, their blocked pressures are significantly reduced to 25 kPa, which is approximately half of the valve's blocked pressure when driven dynamically (Fig. 4*F*).

To summarize, the dynamic DEA soft valve in this work enables high pressure and flow rate control of hydraulic actuators in a compliant and lightweight package. We introduce an ultrahigh-power density DEA and integrate it with a viscoelastic soft channel to achieve voltage-dependent flow and hydraulic pressure regulation. The high-bandwidth valve shows rapid and powerful control of hydraulic actuators of a wide range of volumes. While the dynamic DEA valve we present represents a promising step toward electrical control of soft fluidic

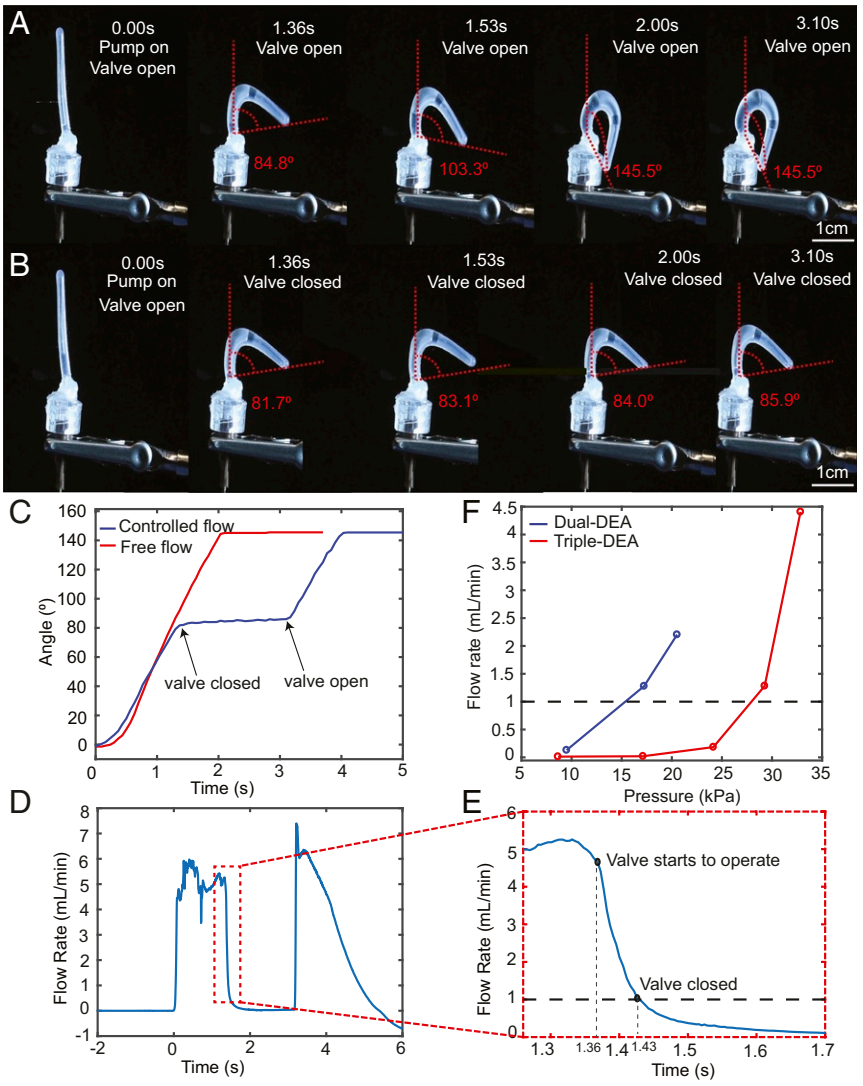

Fig. 4. Demonstration of a dual-DEA valve controlling a small-volume soft actuator. (*A*) Bending motion of the hydraulic actuator with the dual-DEA valve at rest. The actuator takes 1.93 s to reach its maximum bending angle. (*B*) Bending motion of the hydraulic actuator controlled with the dual-DEA valve operated at 1,800 V and 575 Hz. (*C*) Bending angle of the actuator with valve at rest and operated at 1,800 V and 575 Hz corresponding to *A* and *B*, respectively. (*D*) Flow rate of the actuator under DEA valve control corresponding to *B*. (*E*) Controlled flow rate (dashed area in *D*) after the DEA valve is operated. The channel is closed 0.07 s after the valve starts to operate when reaching a flow rate lower than 1 mL·min^{-1}. (*F*) Blocked pressure as a function of flow rate of a dual-DEA and a triple-DEA valve operated quasistatically at 1,000 V.

actuators, there are several aspects to be considered for a future soft onboard control system. The size of the DEA valves in this work was dictated by the size of the mesoscale channels found in macroscale soft actuators. For applications with smaller feature sizes (<100 μm) that require more compact (e.g., microfluidic) designs, we can commensurately reduce the DEA size. To integrate the DEA valve with a soft system, the current rigid supporting frame can be replaced with a soft flexible frame made of materials such as elastomers and 3D printable resins (*Materials and Methods*). More importantly, the current dynamic DEAs use an 1,800-V drive voltage. The associated bulky power supply increases the size and payload requirements for soft robots. Future efforts to reduce the operating voltage (e.g., decreasing the DEA layer thickness) and develop associated compact drive electronics are required to achieve an additional class of lightweight integrated electrical soft fluidic control systems.

Materials and Methods

We fabricate a DEA valve with three steps: DEA fabrication, soft channel casting, and valve assembly. We use an existing multilayering and rolling

Table 2. Material properties

Materials	tan(δ) @ 0.1 Hz	tan(δ) @ 1 Hz	tan(δ) @ 10 Hz	tan(δ) @ 100 Hz	Predicted tan(δ) @ 600 Hz
Ecoflex 0030	0.043	0.077	0.135	0.188	0.220
Elastosil P7670	0.041	0.059	0.082	0.095	0.110
CN9021	0.171	0.316	0.469	0.623	0.800

technique (45) for DEA fabrication and a traditional molding method for the soft channels. We integrate the DEAs and soft channels with both a rigid laser-cut acrylic mechanical frame with metal pins and a soft 5:1 Slygard 184 frame with 3D-printed rods. The DEA soft valve is characterized with a force sensor, a laser displacement measuring tool, a pressure sensor, and a flow rate meter. Detailed fabrication methods are provided in *SI Appendix*.

Data Availability. All study data are included in this article and/or *SI Appendix*.

ACKNOWLEDGMENTS. This work is supported by the National Science Foundation (under awards CMMI-1830291 and EFRI-1830901) and the Wyss Institute for Biologically Inspired Engineering. Any opinions, findings, and conclusions or recommendations expressed in this material are those of the authors and do not necessarily reflect the views of the National Science Foundation.

1. C. Majidi, Soft-matter engineering for soft robotics. *Adv. Mater. Technol.* **4**, 1800477 (2019).
2. E. Brown *et al*., Universal robotic gripper based on the jamming of granular material. *Proc. Natl. Acad. Sci. U.S.A.* **107**, 18809–18814 (2010).
3. R. M. McKenzie, T. W. Barraclough, A. A. Stokes, Integrating soft robotics with the robot operating system: A hybrid pick and place arm. *Front. Robot. AI* **4**, 39 (2017).
4. F. Guan *et al*., Silver nanowire–bacterial cellulose composite fiber-based sensor for highly sensitive detection of pressure and proximity. *ACS Nano* **14**, 15428–15439 (2020).
5. Y. Jin *et al*., "Soft sensing shirt for shoulder kinematics estimation"in *2020 IEEE International Conference on Robotics and Automation (ICRA)* (IEEE, 2020), pp. 4863–4869.
6. X. Ji *et al*., Untethered feel-through haptics using 18-μm thick dielectric elastomer actuators. *Adv. Funct. Mater.* **30**, 2006639 (2020).
7. J. Yang *et al*., Ultrasoft liquid metal elastomer foams with positive and negative piezopermittivity for tactile sensing. *Adv. Funct. Mater.* **30**, 2002611 (2020).
8. A. C. McConnell *et al*., Sophia: Soft orthotic physiotherapy hand interactive aid. *Front. Mech. Eng.* **3**, 3 (2017).
9. P. Brochu, H. Stoyanov, X. Niu, Q. Pei, All-silicone prestrain-locked interpenetrating polymer network elastomers: Free-standing silicone artificial muscles with improved performance and robustness. *Smart Mater. Struct.* **22**, 055022 (2013).
10. S. Li, D. M. Vogt, D. Rus, R. J. Wood, Fluid-driven origami-inspired artificial muscles. *Proc. Natl. Acad. Sci. U.S.A.* **114**, 13132–13137 (2017).
11. C. S. Haines *et al*., New twist on artificial muscles. *Proc. Natl. Acad. Sci. U.S.A.* **113**, 11709–11716 (2016).
12. M. Duduta, E. Hajiesmaili, H. Zhao, R. J. Wood, D. R. Clarke, Realizing the potential of dielectric elastomer artificial muscles. *Proc. Natl. Acad. Sci. U.S.A.* **116**, 2476–2481 (2019).
13. H. Zhao, K. O'Brien, S. Li, R. F. Shepherd, Optoelectronically innervated soft prosthetic hand via stretchable optical waveguides. *Sci. Robot.* **1**, eaai7529 (2016).
14. R. L. Truby *et al*., Soft somatosensitive actuators via embedded 3d printing. *Adv. Mater.* **30**, e1706383 (2018).
15. K. C. Galloway *et al*., Soft robotic grippers for biological sampling on deep reefs. *Soft Robot.* **3**, 23–33 (2016).
16. S. T. Mahon, A. Buchoux, M. E. Sayed, L. Teng, A. A. Stokes, "Soft robots for extreme environments: Removing electronic control"in *2019 2nd IEEE International Conference on Soft Robotics (RoboSoft)* (IEEE, 2019), pp. 782–787.
17. N. R. Sinatra *et al*., Ultragentle manipulation of delicate structures using a soft robotic gripper. *Sci. Robot.* **4**, eaax5425 (2019).
18. M. T. Tolley *et al*., A resilient, untethered soft robot. *Soft Robot.* **1**, 213–223 (2014).
19. P. Polygerinos *et al*., Soft robotics: Review of fluid-driven intrinsically soft devices; manufacturing, sensing, control, and applications in human-robot interaction. *Adv. Eng. Mater.* **19**, 1700016 (2017).
20. M. De Volder, D. Reynaerts, Pneumatic and hydraulic microactuators: A review. *J. Micromech. Microeng.* **20**, 043001 (2010).
21. E. Acome *et al*., Hydraulically amplified self-healing electrostatic actuators with muscle-like performance. *Science* **359**, 61–65 (2018).
22. P. Rothemund, S. Kirkman, C. Keplinger, Dynamics of electrohydraulic soft actuators. *Proc. Natl. Acad. Sci. U.S.A.* **117**, 16207–16213 (2020).
23. T. Ranzani, S. Russo, N. W. Bartlett, M. Wehner, R. J. Wood, Increasing the dimensionality of soft microstructures through injection-induced self-folding. *Adv. Mater.* **30**, e1802739 (2018).
24. V. Cacucciolo *et al*., Stretchable pumps for soft machines. *Nature* **572**, 516–519 (2019).
25. N. W. Bartlett, K. P. Becker, R. J. Wood, A fluidic demultiplexer for controlling large arrays of soft actuators. *Soft Matter* **16**, 5871–5877 (2020).
26. A. Zatopa, S. Walker, Y. Menguc, Fully soft 3d-printed electroactive fluidic valve for soft hydraulic robots. *Soft Robot.* **5**, 258–271 (2018).
27. M. P. Chang, M. M. Maharbiz, Electrostatically-driven elastomer components for user-reconfigurable high density microfluidics. *Lab Chip* **9**, 1274–1281 (2009).
28. L. Yobas, M. A. Huff, F. J. Lisy, D. M. Durand, A novel bulk micromachined electrostatic microvalve with a curved-compliant structure applicable for a pneumatic tactile display. *J. Microelectromech. Syst.* **10**, 187–196 (2001).
29. A. Holke *et al*., An electrostatic, on/off microvalve designed for gas fuel delivery for the MIT microengine. *J. Microelectromech. Syst.* **13**, 660–668 (2004).
30. T. Thorsen, S. J. Maerkl, S. R. Quake, Microfluidic large-scale integration. *Science* **298**, 580–584 (2002).
31. Y. S. Lee, N. Bhattacharjee, A. Folch, 3D-printed Quake-style microvalves and micropumps. *Lab Chip* **18**, 1207–1214 (2018).
32. M. A. Unger, H. P. Chou, T. Thorsen, A. Scherer, S. R. Quake, Monolithic microfabricated valves and pumps by multilayer soft lithography. *Science* **288**, 113–116 (2000).
33. C. Liu, J. Y. Park, Y. Xu, S. Lee, Arrayed ph-responsive microvalves controlled by multiphase laminar flow. *J. Micromech. Microeng.* **17**, 1985 (2007).
34. B. Yang, Q. Lin, A latchable microvalve using phase change of paraffin wax. *Sens. Actuators A Phys.* **134**, 194–200 (2007).
35. R. H. Liu, J. Bonanno, J. Yang, R. Lenigk, P. Grodzinski, Single-use, thermally actuated paraffin valves for microfluidic applications. *Sens. Actuators B Chem.* **98**, 328–336 (2004).
36. C. Yu *et al*., Flow control valves for analytical microfluidic chips without mechanical parts based on thermally responsive monolithic polymers. *Anal. Chem.* **75**, 1958–1961 (2003).
37. M. Kaminaga, T. Ishida, T. Omata, Fabrication of pneumatic microvalve for tall microchannel using inclined lithography. *Micromachines (Basel)* **7**, 224 (2016).
38. P. Rothemund *et al*., A soft, bistable valve for autonomous control of soft actuators. *Sci. Robot.* **3**, eaar7986 (2018).
39. D. J. Preston *et al*., Digital logic for soft devices. *Proc. Natl. Acad. Sci. U.S.A.* **116**, 7750–7759 (2019).
40. M. A. Bell *et al*., Echinoderm-inspired tube feet for robust robot locomotion and adhesion. *IEEE Robot. Autom. Lett.* **3**, 2222–2228 (2018).
41. T. Paschal *et al*., Design, fabrication, and characterization of an untethered amphibious sea urchin-inspired robot. *IEEE Robot. Autom. Lett.* **4**, 3348–3354 (2019).
42. D. McCoul, Q. Pei, Tubular dielectric elastomer actuator for active fluidic control. *Smart Mater. Struct.* **24**, 105016 (2015).
43. M. Giousouf, G. Kovacs, Dielectric elastomer actuators used for pneumatic valve technology. *Smart Mater. Struct.* **22**, 104010 (2013).
44. M. Duduta, R. J. Wood, D. R. Clarke, Multilayer dielectric elastomers for fast, programmable actuation without prestretch. *Adv. Mater.* **28**, 8058–8063 (2016).
45. H. Zhao *et al*., Compact dielectric elastomer linear actuators. *Adv. Funct. Mater.* **28**, 1804328 (2018).
46. Y. Chen *et al*., Controlled flight of a microrobot powered by soft artificial muscles. *Nature* **575**, 324–329 (2019).
47. P. M. Fordyce, C. A. Diaz-Botia, J. L. DeRisi, R. Gomez-Sjoberg, Systematic characterization of feature dimensions and closing pressures for microfluidic valves produced via photoresist reflow. *Lab Chip* **12**, 4287–4295 (2012).
48. A. O'Halloran, F. O'malley, P. McHugh, A review on dielectric elastomer actuators, technology, applications, and challenges. *J. Appl. Phys.* **104**, 9 (2008).
49. R. Pelrine, R. Kornbluh, Q. Pei, J. Joseph, High-speed electrically actuated elastomers with strain greater than 100%. *Science* **287**, 836–839 (2000).
50. T. Lu, C. Ma, T. Wang, Mechanics of dielectric elastomer structures: A review. *Extreme Mech. Lett.* **38**, 100752 (2020).
51. E. Y. Wu, J. Sune, W. Lai, On the Weibull shape factor of intrinsic breakdown of dielectric films and its accurate experimental determination. Part II: Experimental results and the effects of stress conditions. *IEEE Trans. Electron. Dev.* **49**, 2141–2150 (2002).
52. X. Ji *et al*., An autonomous untethered fast soft robotic insect driven by low-voltage dielectric elastomer actuators. *Sci. Robot.* **4**, eaaz6451 (2019).
53. K. P. Becker, Y. Chen, R. J. Wood, Mechanically programmable dip molding of high aspect ratio soft actuator arrays. *Adv. Funct. Mater.* **30**, 1908919 (2020).